Free Form Deformation Method Applied to Modeling and Design of Hypersonic Glide Vehicles

BIN ZHANG, ZHIWEI FENG[ID], BOTING XU[ID], AND TAO YANG

College of Aerospace Science and Engineering, National University of Defense Technology, Changsha 410073, China

Corresponding author: Zhiwei Feng (fzwnudt@163.com)

ABSTRACT The aerodynamic shape of the hypersonic glide vehicle (HGV) has become a research topic nowadays due to its excellent aerodynamic performances. Some limitations need to be reduced when the free-form deformation (FFD) method is applied to parametric modeling and design of an HGV. In this paper, a typical lifting body is considered as an example, and we propose a border-based FFD modeling method that transforms the boundary of FFD lattice into the border of the windward side. Then, the superiority of the border-based FFD modeling method is demonstrated by comparison with the traditional FFD modeling method, and the mesh quality parameters are used to validate the well-deformed model and good geometric continuity of the proposed method. Finally, the border-based FFD modeling method is applied to deformable modeling and aerodynamic simulation of three typical HGV shapes. The results show that the higher efficiency, wider design space, and better applicability are performed by using the border-based FFD modeling method that outperforms the traditional FFD modeling method, and this method we proposed can allow a designer to achieve the better aerodynamic shape of HGVs.

INDEX TERMS Hypersonic gliding vehicle, aerodynamic shape design, parametric modeling, free form deformation, windward side.

I. INTRODUCTION

Hypersonic glide vehicles (HGVs) have become a research topic owing to their high speed, high maneuverability, and high-altitude flight. Unlike traditional aircraft, the body of a HGV provides the main lift force and its aerodynamic shape is characterized by a large windward side [1], aerodisk design [2], thermal protection shield [3], and blunt leading edge [4]. The typical HGV shapes include lifting body [5], blended wing body [6], and waverider body [4], [7]. During the aerodynamic shape design of HGVs, parametric modeling plays a crucial role [8] in determining the performance of the HGV, such as the lift-to-drag ratio (L/D), processing difficulty, ballistic trajectory, stability, and maneuverability. A good parametric modeling method should provide high efficiency, wide design space, and satisfy the design constraints.

Generally, HGVs are capable of atmospheric reentry and unpowered glide; therefore, the aerodynamic shape has an

The associate editor coordinating the review of this manuscript and approving it for publication was Chaoyong Li.

important influence on the HGV's performance. During gliding, the HGV operates with a large angle of attack (AOA) in the initial stage and then maintains an AOA corresponding to the maximum L/D over a long glide distance [9]. Because the windward side of the HGV has the largest contact area with the incoming flow and provides nearly all the lift force, we focus on the parametric modeling of the windward surface in this paper.

There are many studies on parametric modeling of HGVs [1], [6], [10], [11] and common methods include the B-spline method [12], [13], non-uniform rational B-spline (NURBS) method [14], class/shape function transformation (CST) method [15], parametric section (PARSEC) method [16], Hicks-Henne method [17], radial basis function (RBF) method [18], and free form deformation (FFD) method [19]. Among these, the FFD method can be used in arbitrary geometrical models and creates arbitrary theoretical deformation results, thereby providing a wide design space. Most importantly, the FFD method can create new shapes globally or locally and more details can be expressed. In addition, the FFD method can be coupled with mesh

deformation [20], so it is highly suitable for the parametric modeling of the windward surface.

The FFD method was first proposed by Sederberg and Parry [19], who used the Bernstein polynomial as the basis function. The NURBS-based FFD (NFFD) method, which uses the NURBS function as the basis function, was proposed by Lamousin and Waggenspaek [21]. An extended FFD (EFFD) method was proposed by Coquillart [22] to model complex geometry. Hsu *et al.* [23] proposed the direct manipulation of the FFD (DFFD) method, which directly and accurately manipulates the geometry. Subsequently, Feng *et al.* [24] introduced the shape surface and height surface methods to the FFD method for surface deformation, and Yoon and Kim [25] proposed a sweep-based FFD method. The FFD method has been widely used for the aerodynamic shape design of aircraft. For example, Gagnon and Zingg [26] transformed a spherical shape into the shape of the aircraft using a two-level FFD method, Zhang *et al.* [11] conducted a review of the FFD method for aerodynamic design, and Koo and Zingg [27] optimized a rectangular wing and various wingtip treatments using the FFD method.

However, current researches on FFD method mostly focused on traditional aircraft, such as airfoils and wings. Few studies have considered HGV shapes. In our work, we found that several problems limit the current FFD method for well parametric modeling of the HGV, such as the large computational complexity, low operational efficiency, and geometric discontinuity. In order to solve these problems, a border-based FFD modeling method is presented in this study and it is demonstrated that the proposed method is well-suited for modeling and design of the HGV.

This paper is organized as follows. The next section introduces the FFD methods with NURBS basis function. In Section 3, we propose some limitations yet to be solved when applied the FFD method to the parametric modeling of windward side. In Section 4, we introduce a border-based control surface and develop the border-based FFD modeling procedure. Section 5 validates the superiority and applicability of the border-based FFD modeling method. Section 6 completes the paper with the conclusion.

II. FREE FORM DEFORMATION
In FFD method, the to-be-deformed geometry is inserted into an elastic FFD control lattice and the mapping relation between the geometric mesh points and control points are created. When the control points move, the geometric model will be deformed based on the mapping relationship. We use a typical lifting body as an example to describe the FFD method, as shown in Fig. 1.

A. FFD CONTROL LATTICE
In FFD method, a parallel hexahedron is commonly used as the control lattice. The control lattice contains the to-be-deformed geometry. We use the lifting body as an example and create an isometric cuboid control lattice, which consists
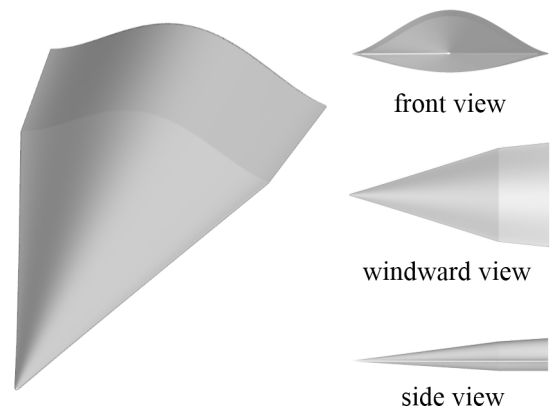

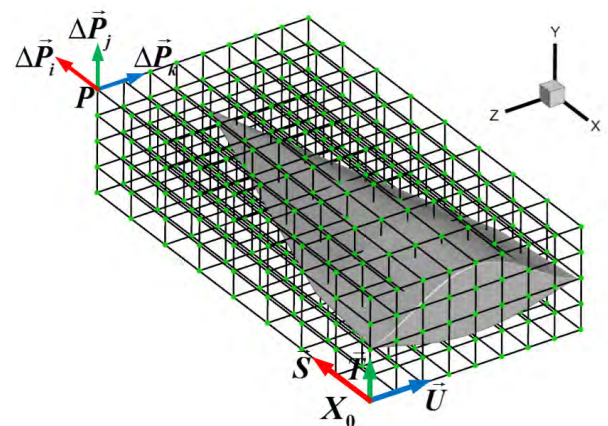**FIGURE 1.** The geometric model of a typical lifting body.

FIGURE 2. The cuboid control lattice and local coordinate system.

of the green control points and black lattices, as shown in Fig. 2.

B. LOCAL COORDINATE SYSTEM
Based on the cuboid control lattice, the local coordinate system X_0-STU is created. The origin of the local coordinate system is X_0 and the axial vectors along the directions of the length, height, and width of the control lattice are $\vec{S}$, $\vec{T}$, and $\vec{U}$. Using the local coordinate system, any geometric mesh point $\vec{X}$ can be described as

$$\vec{X} = \vec{X}_0 + s\vec{S} + t\vec{T} + u\vec{U} \tag{1}$$

where s, t, u $(0 \leq s, t, u \leq 1)$ are the local coordinates of $\vec{X}$.

C. FFD CONTROL POINT
The number of FFD control points along the axial vectors of $\vec{S}$, $\vec{T}$, and $\vec{U}$ are $(l+1)$, $(m+1)$, and $(n+1)$ respectively. As Fig. 2 shows, we use $l = 8$, $m = 4$, and $n = 8$. Any control point $\vec{P}_{i,j,k}$ can be chosen as the design control point, which is defined as

$$\vec{P}_{i,j,k} = \vec{X}_0 + \frac{i}{l}\vec{S} + \frac{j}{m}\vec{T} + \frac{k}{n}\vec{U} \tag{2}$$

where $\vec{P}_{i,j,k}$ is the global coordinate of the design control point; i, j, and k $(i = 0, 1, \cdots, l; j = 0, 1, \cdots, m;$

$k = 0, 1, \cdots, n$) are the sequences of the control points along the axial vectors of $\vec{S}$, $\vec{T}$, and $\vec{U}$.

D. MAPPING RELATIONSHIP

The mapping relationship between the geometric mesh points $\vec{X}$ and control points $\vec{P}_{i,j,k}$ is the key in FFD method. Based on the basis function $R(\cdot)$, the mapping relationship is generally written as

$$\vec{X} = \sum_{i=0}^{l} \sum_{j=0}^{m} \sum_{k=0}^{n} R_i(s)R_j(t)R_k(u) \cdot \vec{P}_{i,j,k} \qquad (3)$$

where $R_i(s)$, $R_j(t)$, and $R_k(u)$ are the basis functions along the axial vectors of $\vec{S}$, $\vec{T}$, and $\vec{U}$.

The basis function $R(\cdot)$ plays an important role in the mapping relationship. The Bernstein polynomial, B-Spline function, and NURBS function are the commonly used basis functions. Because the NURBS function introduces an additional weight factor to enable a wide design space [28], we use the NFFD method in this study.

E. DEFORMATION OF GEOMETRIC MODEL

The deformation of the geometry is manipulated by moving the design control point $\vec{P}_{i,j,k}$; the displacement changes $\Delta\vec{P}_i$, $\Delta\vec{P}_j$, and $\Delta\vec{P}_k$ are along the axial vectors of $\vec{S}$, $\vec{T}$, and $\vec{U}$, as shown in Fig. 2. Based on the mapping relationship and NURBS basis function, the displacement change $\Delta\vec{X}$ of the geometric mesh point $\vec{X}$ can be defined as

$$\Delta\vec{X} = \sum_{i=0}^{l} \frac{\omega_i N_{i,p}(s)}{\sum\limits_{a=0}^{l} \omega_a N_{a,p}(s)} \left(\sum_{j=0}^{m} \frac{\omega_j N_{j,q}(t)}{\sum\limits_{b=0}^{m} \omega_b N_{b,q}(t)} \right.$$
$$\left. \times \left(\sum_{k=0}^{n} \frac{\omega_k N_{k,r}(u)}{\sum\limits_{c=0}^{n} \omega_c N_{c,r}(u)} \cdot \Delta\vec{P}_{i,j,k} \right) \right) \qquad (4)$$

where p, q, and r are the orders of the NURBS basis function and ω_i, ω_j, and ω_k are the weight factors of the design control point.

III. LIMITATIONS OF THE FFD METHOD

Though there are many advantages of the FFD method, such as geometric independence, random deformation, and mesh synchronization, current research has mainly focused on traditional vehicles [29]. At present, few studies have been conducted on the parametric modeling of the HGVs using the FFD method; therefore, we focus on this topic in this paper. During the study, we found the following problems that have yet to be solved.

A. LARGE COMPUTATIONAL COMPLEXITY

In general, there are millions of geometric mesh points and hundreds of control points need to be moved during the FFD modeling of the windward side. In addition, in theory,

there are displacement changes in three directions for each control point; therefore, the computational complexity of the mapping and reverse mapping between the control points and mesh points is very high. For example, there are 405 control points and each one has 3 displacement changes in Fig. 2, which results in 3×405 theoretical variables. The mapping operation includes three nested levels due to three dimensions of the FFD control lattice, so this results in a time complexity of $3 \times O(405^3)$.

Besides the mapping operation, a high computational cost is associated with solving the local coordinates of the geometric mesh points. It is relatively simple to solve the local coordinates for the isometric cuboid displayed in Fig. 2. However, for an irregular FFD control lattice, complex mathematical methods are needed to solve the local coordinates [22], thereby further increasing the calculation time.

The aerodynamic shape design of an HGV is rather time-consuming; therefore, one of our objectives is to simplify the FFD modeling and reduce the calculation complexity.

B. LOW OPERATIONAL EFFICIENCY

As mentioned before, the to-be-deformed geometry is inserted into a control lattice. When the control lattice has a regular structure, part of the control points that are projected in the $X_0 - SU$ plane must be outside of the windward side. However, only the projected points within the windward side can be used as a design control points whereas the other projected points can only be used as non-design control points.

Therefore, for a regular control lattice, the design control points have to be selected before the FFD modeling begins. In addition, when the geometric model is updated or the control lattice is modified, the design control points have to be re-selected, which results in low operational efficiency.
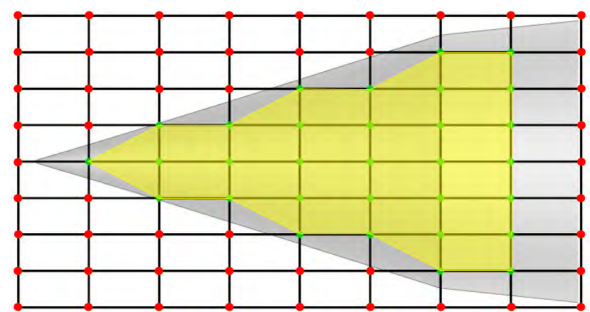

FIGURE 3. Control points are projected in $X_0 - SU$ plane of the control lattice.

As shown in Fig. 3, the control points are projected in $X_0 - SU$ plane of the control lattice; the green points within the windward side are design control points, the red points outside the windward side are non-design control points, and the yellow region is the operating region for the FFD modeling of the windward side.

The red non-design control points account for 62% of all control points, exceeding the proportion of the green design control points, which account for 38%. This indicates
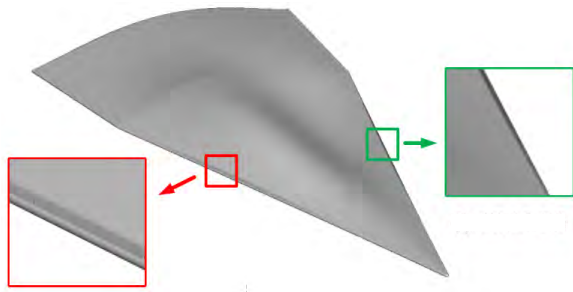
FIGURE 4. The geometric discontinuity of the FFD modeling results of the HGV.

that the number of design points is less than non-design control points. Moreover, as the design control points increase, the non-design control points also increase proportionately.

When conducting FFD modeling of the windward side, we want to avoid the selection of design control points and also reduce the proportion of non-design control points. Therefore, another objective of the study is to increase operational efficiency.

C. GEOMETRIC DISCONTINUITY

The FFD modeling of the windward side is a local modeling approach; therefore, it is important to ensure the geometric continuity between the deformable region and the non-deformable region. In this study, we want to ensure the geometric continuity between the windward side and the leading edge of the HGV. The windward side is a smooth surface with small curvature but the leading edge is a blunt surface

with large curvature. As a result, geometric discontinuity at the edge is common, as shown in Fig. 4.

When geometric discontinuity occurs, the geometric integrity of the model is compromised and the FFD modeling fails. Therefore, we have to ensure that the deformation of the windward side occurs in a suitable region. Currently, the most common method to ensure local deformation is the EFFD method, which uses several parallel hexahedrons as the control lattices. In other researches, spliced hexagonal pyramids [30] and complex Bezier tetrahedron [31] have also been used as EFFD control lattices. By integrating several smaller control lattices into a single large control lattice, the EFFD method allows for local deformation.

However, the EFFD method achieves local deformation by complicating the structural simplicity of the FFD control lattice, which not only requires additional constraint equations to ensure the continuity among different control lattices but also requires the coordination of several control lattices in one-time modeling. If the EFFD method is used, the computational complexity and operational difficulty are increased; therefore, a simpler method should be developed.

IV. BORDER-BASED FFD CONTROL SURFACE

In order to solve the above-mentioned limitations, we made several improvements on the traditional FFD control lattice and proposed a border-based FFD control surface. The details of the method are described in the following sections.

A. REDUCTION OF THE DIMENSIONS

As a universal parametric modeling method, the traditional FFD control lattice has a regular three-dimensional (3D)
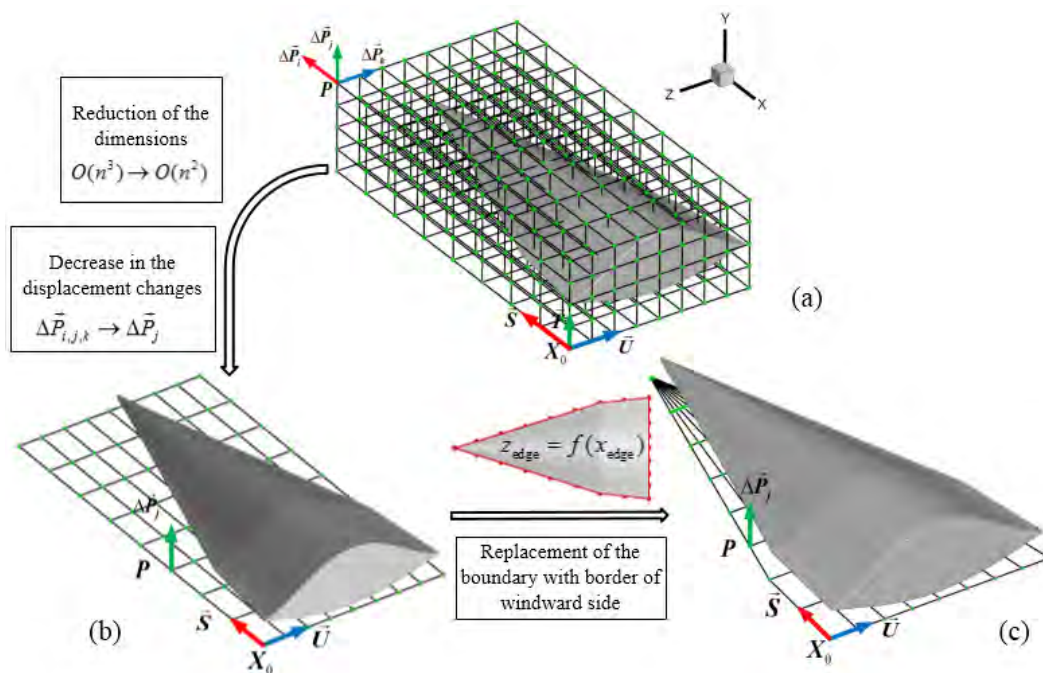
FIGURE 5. The transition process of the FFD control lattice, first simplify the (a) 3D isometric cuboid control volume as a (b) 2D rectangular control surface, and then replace the boundary of the regular control surface with the projected border of $z_{edge} = f(x_{edge})$ to get the (c) 2D border-based control surface.
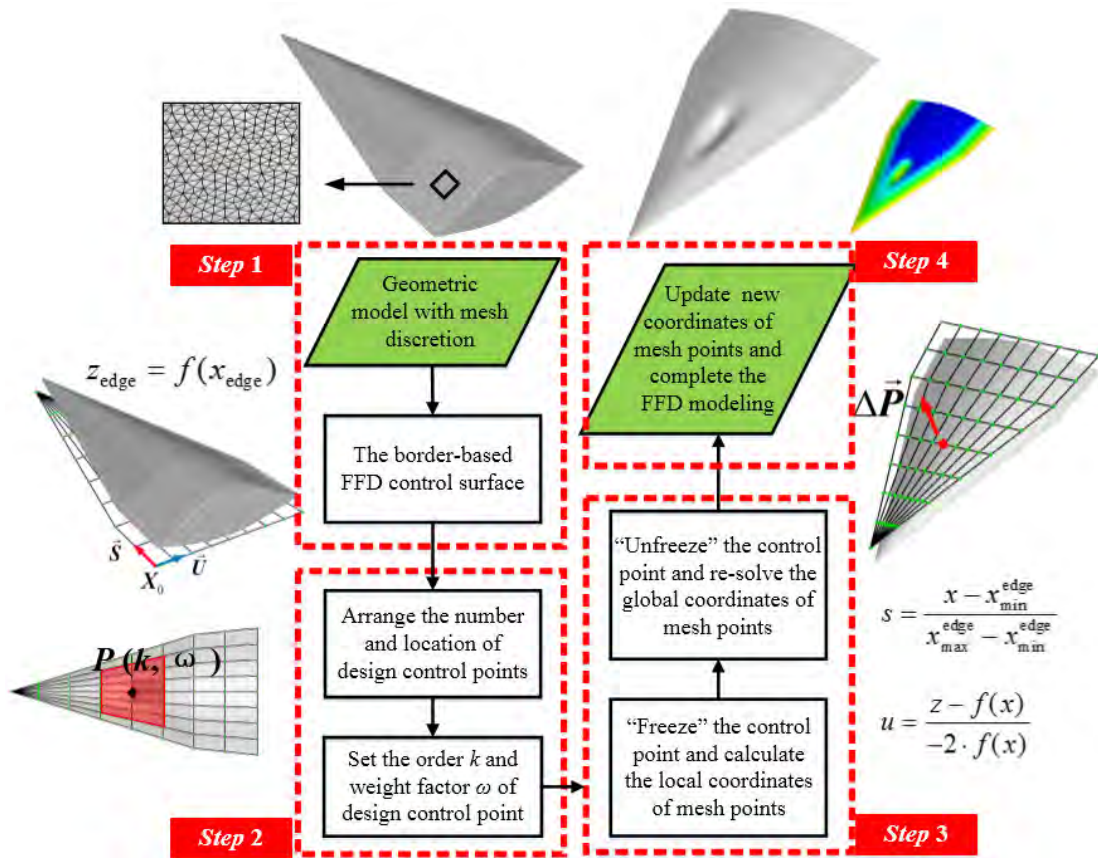
FIGURE 6. The flowchart of the border-based FFD modeling procedure on the windward side of a HGV.

structure, such as the isometric cuboid shown in Fig. 2. However, since the windward side of the HGV has a smooth surface, the traditional 3D control volume can be simplified as a two-dimensional (2D) rectangular control surface, as shown in the transition from Fig. 5(a) to Fig. 5(b). Based on the local coordinate system X_0-STU, the 2D control surface is located in the $X_0 - SU$ plane, the axial vectors are $\vec{S}$ and $\vec{U}$, and the origin remains at X_0, as shown in Fig. 5(b).

B. DECREASE IN THE DISPLACEMENT CHANGES

According to the geometric characteristics of the windward side, the design space of the HGV is concentrated in the $\vec{T}$ direction. Therefore, we only need to manipulate the displacement changes of design control points in the $\vec{T}$ direction. As Fig. 5 (b) shows, we use the displacement change $\Delta\vec{P}_j$ of any control point P in the $\vec{T}$ direction as the design variable to decrease the displacement changes from $\Delta\vec{P}_{i,j,k}$ to $\Delta\vec{P}_j$.

C. REPLACEMENT OF THE BOUNDARY

By reducing the dimensions of the control lattice and decreasing the displacement changes of the control points, the 2D control surface has been simplified. In order to satisfy the design requirements, we first extract the projected border of the windward side in the $X_0 - SU$ plane; the curves of the

TABLE 1. Comparison of the computational complexity of the FFD modeling methods.

	border-based surface	traditional lattice
number of dimensions	2	3
number of total control points	81	405
displacement changes of each control point	1	3
computational complexity	$O(81^2)$	$3 \times O(405^3)$

projected border are $z_{edge} = f(x_{edge})$. Then we replace the boundary of the regular control surface with the projected border of $z_{edge} = f(x_{edge})$, as shown in the transition from Fig. 5(b) to Fig. 5 (c). The coordinates of the geometric mesh points on the windward side are (x, y, z); the local coordinate values of the mesh points can be calculated as

$$s = \frac{x - x_{\min}^{\text{edge}}}{x_{\max}^{\text{edge}} - x_{\min}^{\text{edge}}}, \quad u = \frac{z - f(x)}{-2 \cdot f(x)} \quad (5)$$

where s and $u(0 \le s, u \le 1)$ are the local coordinate values of the mesh point, x and z are the global coordinate values of the mesh point, x_{edge} and z_{edge} are the global coordinate values of the curves on the projection border, $x_{\min}^{\text{edge}}$ is the minimum value of x_{edge}, and $x_{\max}^{\text{edge}}$ is the maximum value of x_{edge}.

On the border-based control surface, the displacement changes $\Delta\vec{P}_j$ only occur in the $\vec{T}$ direction for all design
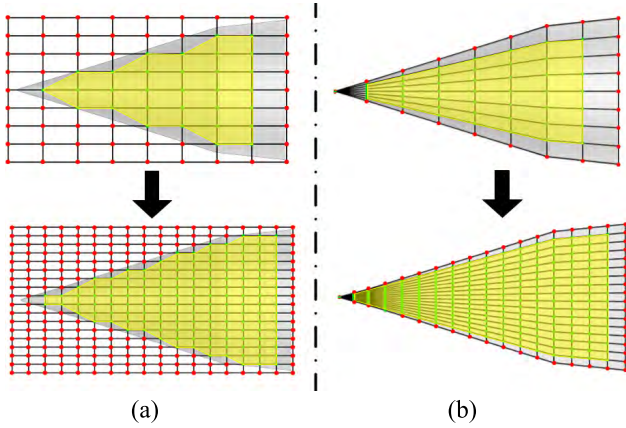
(a)   (b)

FIGURE 7. The projections in the $X_0 - SU$ plane of the (a) traditional control volume and (b) border-based control surface.

TABLE 2. The proportions of the design control points for different control lattices.

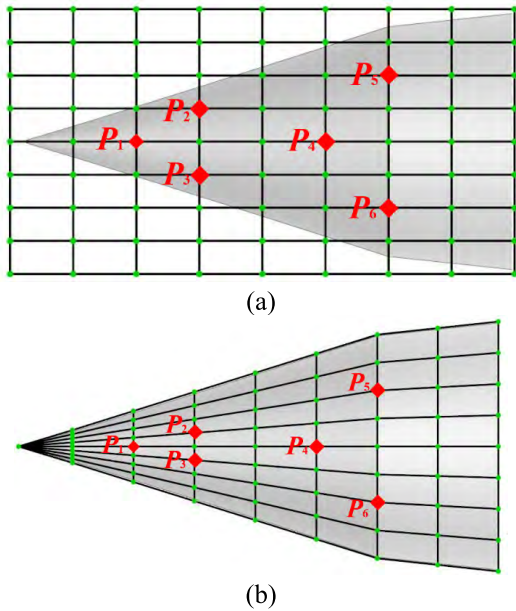| number of control points	border-based surface	traditional volume
81 (9×9)	60%	38%
324 (18×18)	79%	45%
∞	close to 100%	less than 60%

(a)

(b)

FIGURE 8. The positional distribution of six design control points on (a) traditional control volume and (b) border-based control surface.

control points and the displacement changes $\Delta \vec{y}$ of all mesh points on the windward side are defined as

$$\Delta \vec{y} = \sum_{i=0}^{l} \frac{\omega_i N_{i,p}(s)}{\sum_{a=0}^{l} \omega_a N_{a,p}(s)} \left(\sum_{k=0}^{n} \frac{\omega_k N_{k,r}(u)}{\sum_{c=0}^{n} \omega_c N_{c,r}(u)} \cdot \Delta \vec{P}_j \right) \quad (6)$$

TABLE 3. The sequences and displacement changes of six design control points.

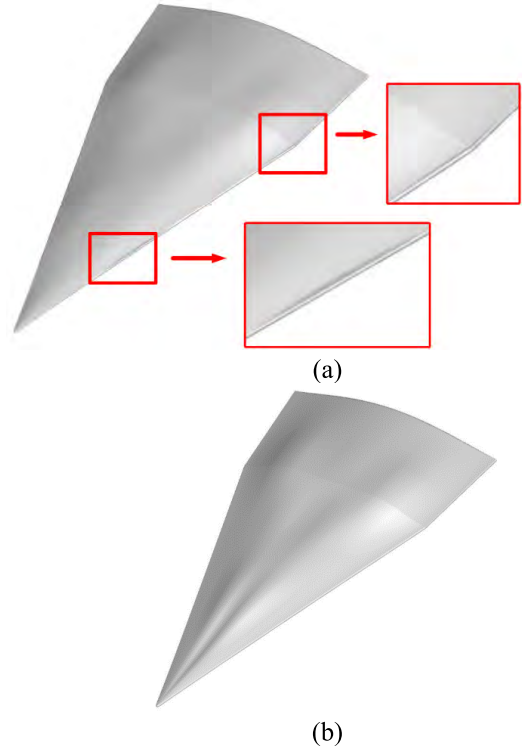|	P_1	P_2	P_3	P_4	P_5	P_6
i	4	5	3	4	6	2
j	0	0	0	0	0	0
k	6	5	5	3	2	2
$\Delta \vec{P}$	2.0	-4.0	-4.0	6.0	-8.0	-8.0

(a)

(b)

FIGURE 9. Deformation results of the windward side based on (a) traditional control volume and (b) border-based control surface.

D. MODELING PROCEDURE

The flowchart of the border-based FFD modeling procedure integrated with the NURBS basis function is shown in Fig. 6. The key steps are introduced as follows.

Step 1: Based on the geometric model with mesh discretion, we first set up the local coordinate system $X_0 - SU$. Then the projected border of the windward side in the $X_0 - SU$ plane is defined as $z_{\text{edge}} = f(x_{\text{edge}})$. Next, we replace the boundary of the regular control lattice with the border of windward side. For simplicity, we can ensure that the control point with a single displacement of $\Delta \vec{P}_j$ changes only in the $\vec{T}$ direction.

Step 2: The number and location of the design control points are arranged based on the design requirements. In the NURBS basis function, the order k controls the deformation range and the weight factor ω controls the deformation degree. In addition, we can set the order k and weight factor ω
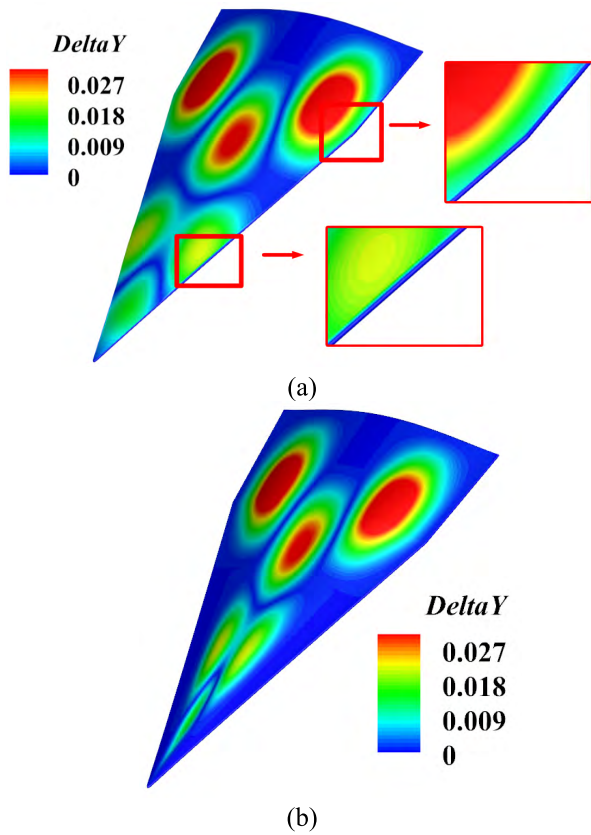
FIGURE 10. Contours of the coordinate changes Delta Y on the windward side for (a) traditional control volume and (b) border-based control surface.

of an arbitrary design control point to satisfy the design requirements.

Step 3: The mapping relationship between the control points and mesh points is conducted after step 2. This process involves the transformation between the local and global coordinate systems, which is performed using the "Freeze" and "Unfreeze" operations. First, we do not change the coordinates of the design control points to calculate the local coordinates of the mesh points; this is referred to as the "Freeze" operation. Then we manipulate the design control point P with the displacement change $\Delta \vec{P}_j$ and solve the global coordinates again by reverse mapping; this is referred to as the "Unfreeze" operation.

Step 4: Based on the mapping relationship, the new coordinates of the mesh points on the windward side are updated after step 3. This step completes the FFD modeling and a new geometric model is created. Subsequently, this modeling procedure can be operated iteratively according to the design objects.

V. RESULTS AND DISCUSSION
A. COMPARISONS
We compared the border-based FFD modeling method with the traditional FFD modeling method to demonstrate the superiorities of the border-based control surface, such as the
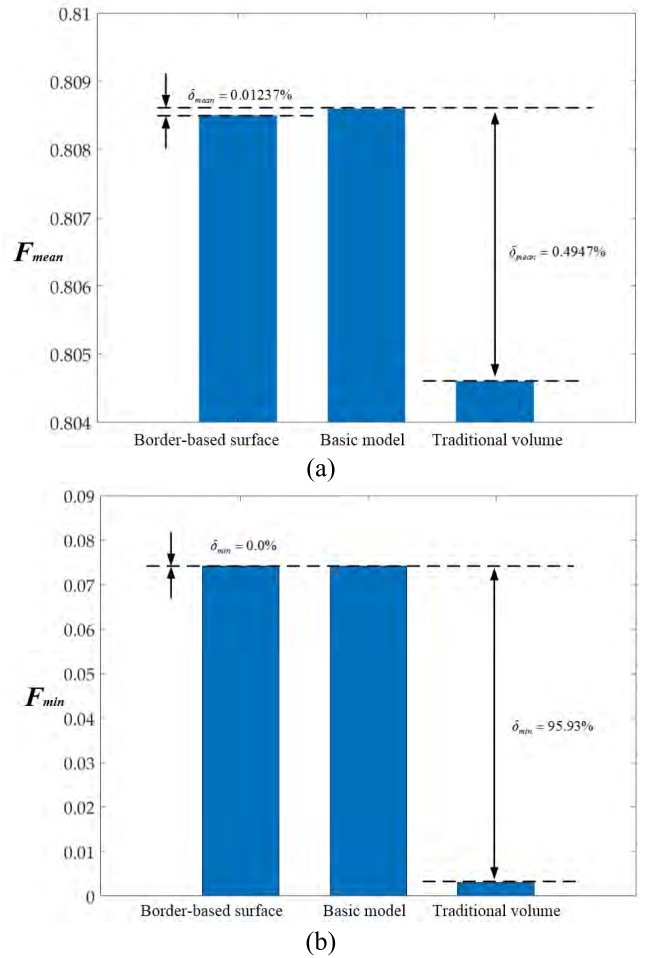

FIGURE 11. The comparisons of the (a) average mesh quality and (b) minimum mesh quality of the basic model and the different deformed models.

lower computational complexity, the high operational efficiency, and good geometric continuity.

1) LOWER COMPUTATIONAL COMPLEXITY
First, the dimensions of the FFD control lattice were reduced from three to two; therefore, the mapping process has only two nested levels. The time complexity has been reduced from $O(n^3)$ to $O(n^2)$. Second, due to the reduction of the dimensions, the total number of control points also has been reduced. In addition, the displacement changes of the design control points are further simplified.

We use the lifting body as an example; the design control points only have one displacement change in $\vec{T}$ direction, which reduces the time complexity from $3 \times O(405^3)$ to $O(81^2)$. The detailed results are listed in Table 1; the computational complexity has been reduced significantly by the border-based FFD modeling method.

2) INCREASE IN OPERATIONAL EFFICIENCY
The projections in the $X_0 - SU$ plane of the traditional control volume and the border-based control surface are shown
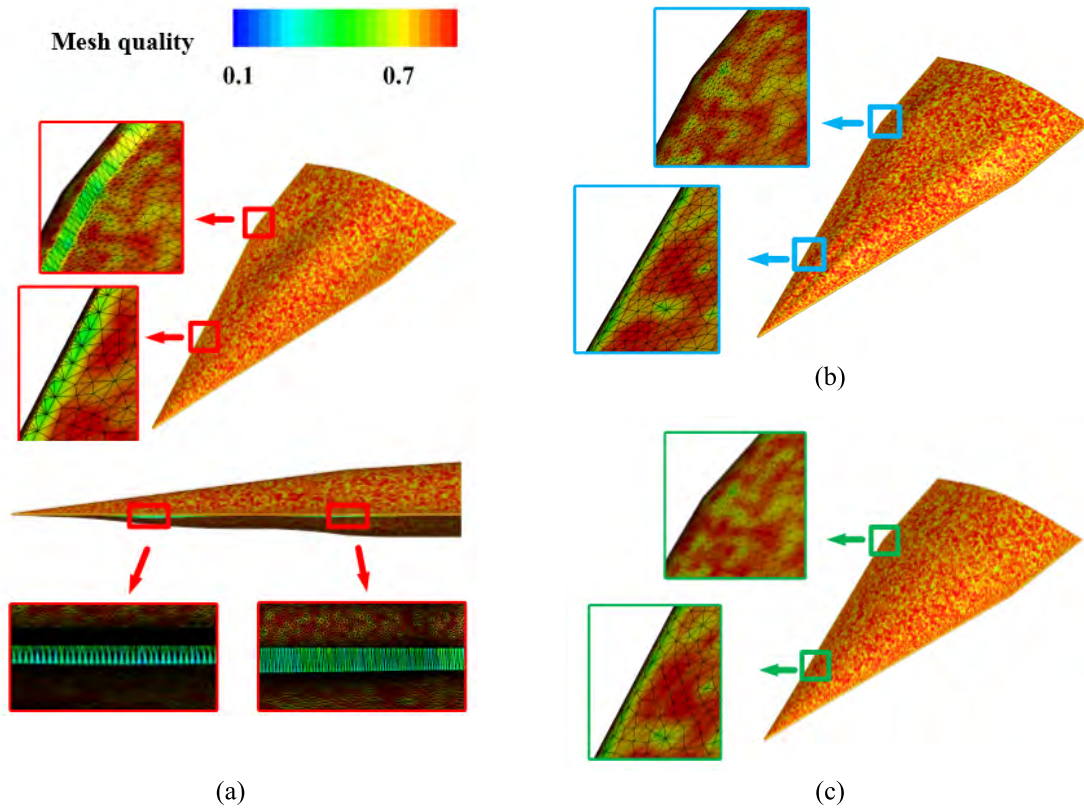
FIGURE 12. Contours of the mesh quality of the deformed models obtained from (a) traditional control volume and (b) border-based control surface, and contour of the mesh quality of the (c) basic model.

in Fig. 7 (a) and (b), respectively. For both FFD modeling methods, the number of control points in the bottom lattice (that is 18 × 18) is four times that of the top lattice (that is 9 × 9). The green points are the design control points, the red points are the non-design control points, and the yellow region is the operating region for the FFD modeling of the windward side.

The comparison of Fig. 7(a) and Fig. 7(b) indicates that many non-design control points exist in the traditional control volume but in the border-based control surface, nearly all the control points can be used as design points, except for the points on the outermost border. In the top panel of Fig. 7, the number of control points is 9 × 9 for both control lattices; the proportion of the design control points is 38% for the traditional control volume and 60% for the border-based control surface. In the bottom panel of Fig. 7, the proportion of design control points is 45% for the traditional control volume and 79% for the border-based control surface.

In theory, the maximum proportion of the design control points for the traditional control volume is less than the area ratio of the projected windward side to the $X_0 - SU$ plane in the control volume (the area ratio is 60% in Fig. 7), but the maximum proportion of the design control points for the border-based control surface can approach 100%. The proportions of the design control points for the different control lattices are shown in Table 2.

It is evident that the proportion of the design control points is larger for the border-based control surface than the traditional control volume and that this proportion increases as the control points increased. Furthermore, the selection procedure of the design control points is not required in the border-based control surface. The results show that the operational efficiency is increased by the border-based FFD modeling method.
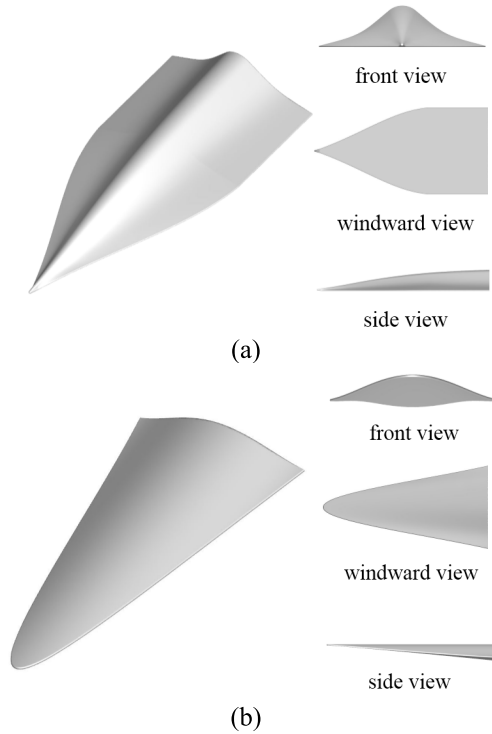
3) GOOD GEOMETRIC CONTINUITY
Because the edge that connects the windward side and leading edge is the area where the geometric discontinuity occurs, the deformed region must be limited within the windward side. An inherent advantage of the border-based FFD modeling method is the geometrical similarity between the boundary of the control surface and the border of the windward side. During the FFD modeling, we set the control points on the outermost border as non-design control points. Because there are no deformation at the boundary of the control surface and the deformation is limited within the windward side, so the border-based control surface can ensure geometric continuity in theory.

In order to verify the geometric continuity, we choose six design control points $P_1 \sim P_6$ on the traditional control volume and border-based control surface, as shown in Fig. 8. The sequences (i, j, k) in the local coordinate system of the

TABLE 4. Mesh qualities of basic model and deformed models with different control lattices.

	F_{mean}	F_{min}	δ_{mean}	δ_{min}
basic model	0.8086	0.07416	0%	0%
border-based surface	0.8085	0.07416	0.012%	0%
traditional volume	0.8046	0.003015	0.49%	95.93%

FIGURE 14. The border-based control surfaces on the windward sides of (a) lifting body, (b) blended wing body, and (c) waverider body.

FIGURE 13. Two typical HGV shapes of (a) blended wing body, and (b) waverider body.
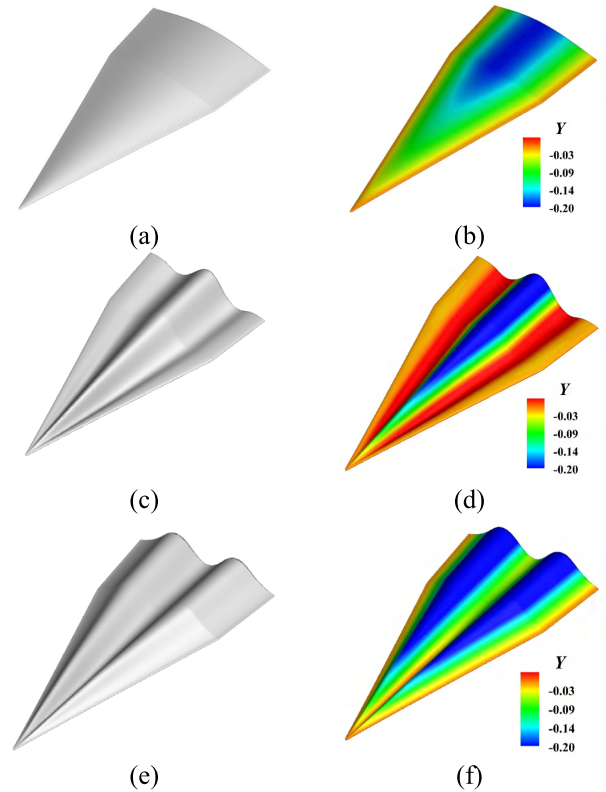
FIGURE 15. Models of the lifting body: (a) basic lifting body, (c) deformed lifting body A, and (e) deformed lifting body B, and the contours of the *Y* coordinates on the windward sides: (b) basic lifting body, (d) deformed lifting body A, and (f) deformed lifting body B.

design control points are the same in both two control lattices. The sequences (i, j, k) of $P_1 \sim P_6$ and their displacement changes $\Delta \vec{P}$ are listed in Table 3.

During FFD modeling of the windward side, the displacement changes of the design control points are $\Delta \vec{P} = (2.0, -4.0, -4.0, 6.0, -8.0, -8.0)$, the weight factors of the design control points are $\omega = (4, 6, 6, 6, 6, 6)$, and the order of NURBS basis function is $k = 2$. The deformation results of the windward side are shown in Fig. 9 and the contours of the coordinate changes Delta *Y* on the windward side are shown in Fig. 10.

Fig. 9(a) and Fig. 10(a) indicate that there are at least two regions of geometric discontinuity in the traditional control volume method; these are magnified in the red boxes. However, there are no geometric discontinuities observed in Fig. 9(b) and Fig. 10(b); the coordinate changes Delta *Y* are all on the windward side and no *Y* coordinate changes occur near the edges.

The comparisons demonstrate that for the same displacement changes of the design control points and basis function,

the border-based control surface ensures geometric continuity and the deformation is limited within the windward side. More importantly, unlike the EFFD method that uses multiple FFD control lattices with additional constraints, the border-based FFD modeling method achieves similar local deformation with no constraints.

B. MESH QUALITY

Because the FFD method directly manipulates the geometric mesh points, we investigate the mesh quality parameters [32] to evaluate the robustness of the deformation models.

Discretized by the triangle mesh element, we first define the change in the element's size f_{size}^{2D} as:

$$f_{size}^{2D} = \min(\tau, \frac{1}{\tau}) \qquad (7)$$
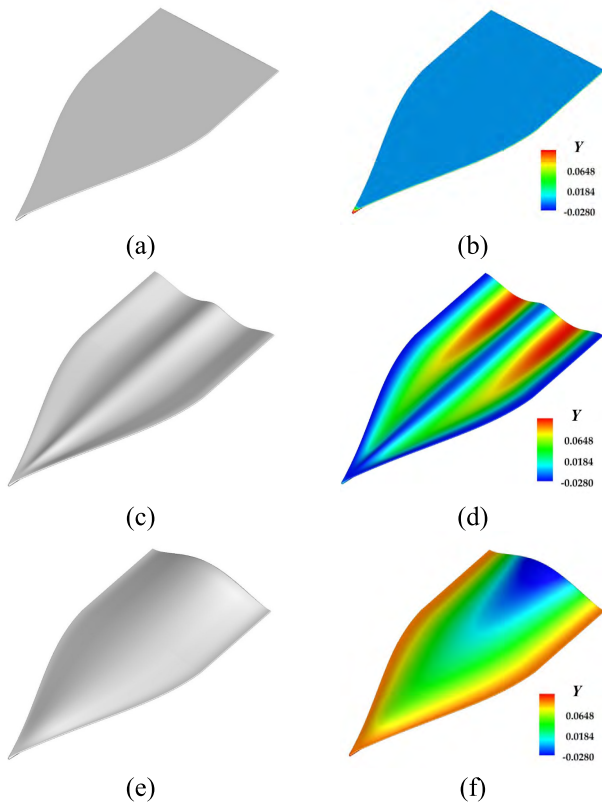
FIGURE 16. Models of the blended wing body: (a) basic blended wing body, (c) deformed blended wing body A, and (e) deformed blended wing body B, and the contours of the Y coordinates on the windward sides: (b) basic blended wing body, (d) deformed blended wing body A, and (f) deformed blended wing body B.

FIGURE 17. Models of the waverider body: (a) basic waverider body, (c) deformed waverider body A, and (e) deformed waverider body B, and the contours of the Y coordinates on the windward sides: (b) basic waverider body, (d) deformed waverider body A, and (f) deformed waverider body B.

where τ is the area ratio defined as:

$$\tau = \frac{S}{\varsigma} \qquad (8)$$

where S is the area of the mesh element, and ς is the area of an equilateral triangle comprised of the second side length of the element.

Second, the change in the element's shape f^{2D}_{shape} can be described as:

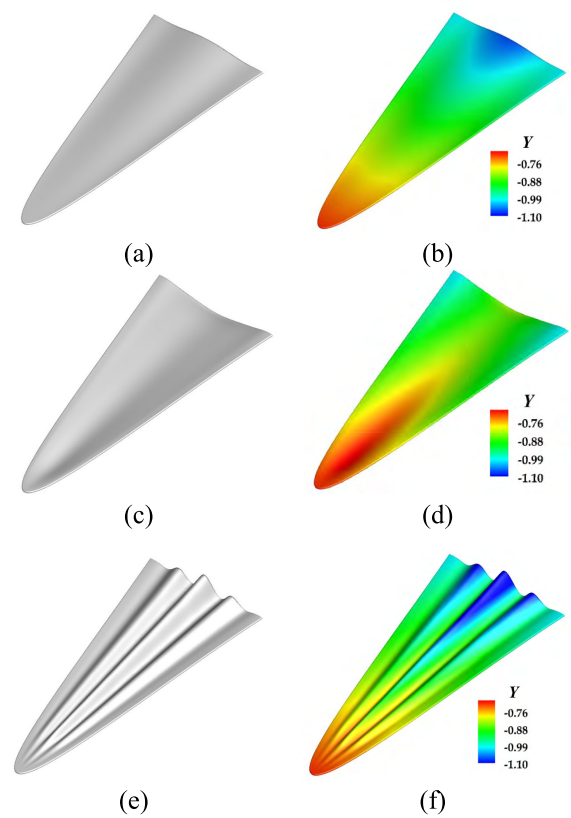$$f^{2D}_{shape} = \frac{4\sqrt{3}S}{\sum\limits_{i=1}^{3} l_i^2} \qquad (9)$$

where $l_i(i = 1, \cdots, 6)$ are the sides of a triangular element.

Thus, the changes in the size and shape represent the measure of mesh quality, which is defined as:

$$f^{2D}_{size-shape} = f^{2D}_{size} \cdot f^{2D}_{shape} \qquad (10)$$

where $f^{2D}_{size-shape} \in (0, 1]$ and when the element's quality is better, $f^{2D}_{size-shape} \to 1$.

Finally, by determining the parameter $f_{size-shape}$ for each element, we can obtain the average value of $f_{size-shape}$ of all elements as F_{mean} and the minimum value as F_{min}, which are

given by:

$$\begin{cases} F_{mean} = \dfrac{\left(\sum\limits_{i=1}^{Ne} f^i_{size-shape}\right)}{Ne} \\ F_{\min} = \min\left(f^1_{size-shape}, f^2_{size-shape}, \cdots, f^{Ne}_{size-shape}\right) \end{cases} \qquad (11)$$

where Ne is the number of mesh elements.

In order to evaluate the descend range of the mesh quality parameters, we use a quantitative evaluation formula:

$$\delta = \frac{F_{Base} - F_{FFD}}{F_{Base}} \times 100\% \qquad (12)$$

where δ is the descend range of the mesh quality, F_{Base} is the mesh quality of the windward side with no deformation and F_{FFD} is the mesh quality of the deformed windward side using the FFD method. In this study, the smaller the value of δ, the higher the mesh quality of the deformed model is and the better the control lattice method is.

The comparisons of the mesh quality of the basic model and the deformed models are presented in Fig. 11, and the detailed results are shown in Table 4. The mesh quality of the deformed model with the border-based control surface is close to that the basic model; the descend range value is 0.01237% for the average mesh quality and no change for the minimum mesh quality. The descend range of average mesh
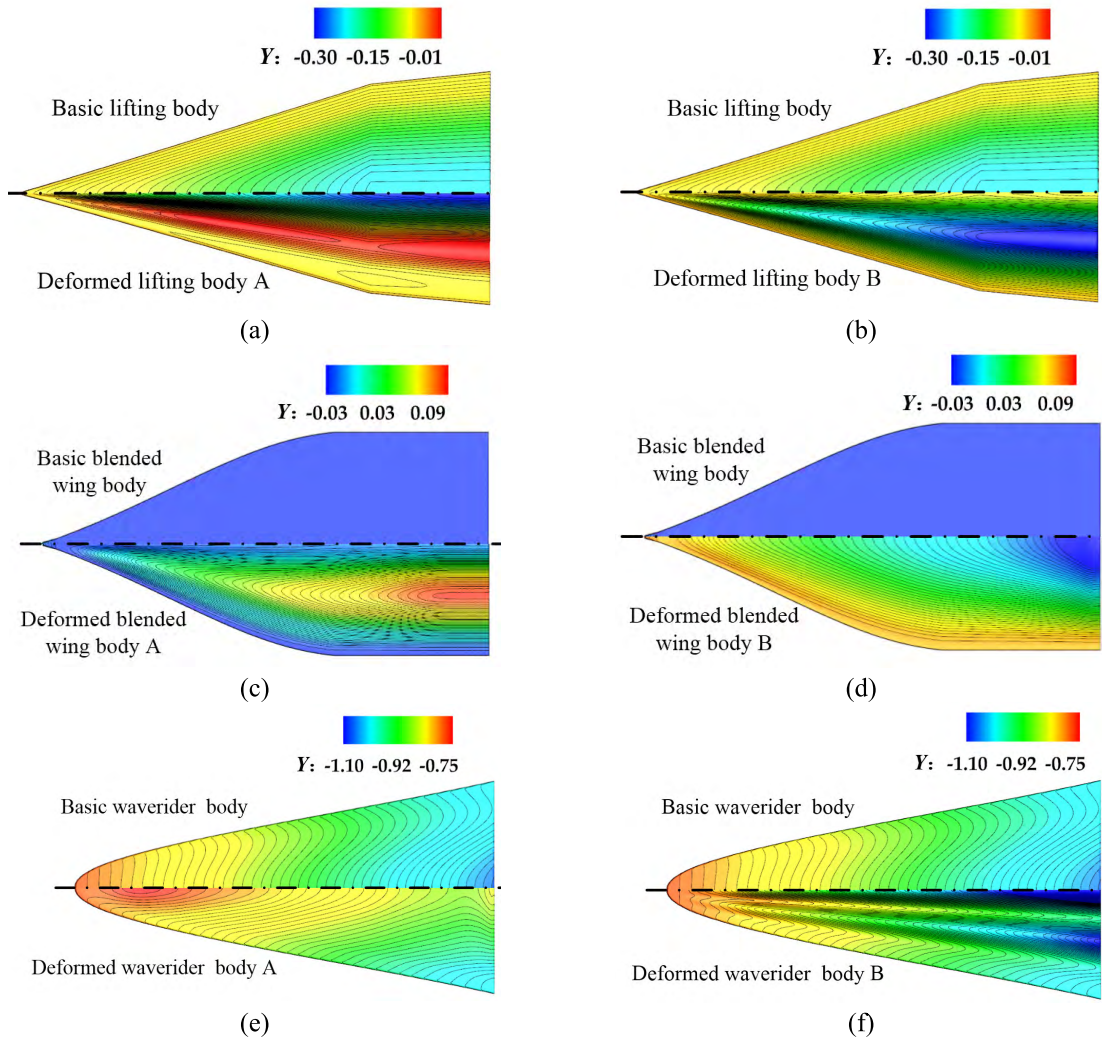
FIGURE 18. The comparative contours of the *Y* coordinates on the windward sides: (a) basic lifting body and deformed lifting body A, (b) basic lifting body and deformed lifting body B, (c) basic blended wing body and deformed blended wing body A, (d) basic blended wing body and deformed blended wing body B, (e) basic waverider body and deformed waverider body A, (f) basic waverider body and deformed waverider body B.

TABLE 5. The aerodynamic results of the HGVs.

	lifting body			blended wing body			waverider body		
	Base	A	B	Base	A	B	Base	A	B
C_A	0.04	0.02	0.06	0.01	0.01	0.06	0.06	0.03	0.07
C_N	0.38	0.31	0.38	0.39	0.35	0.60	0.60	0.50	0.65
C_L	0.37	0.31	0.37	0.39	0.35	0.59	0. 36	0.49	0.63
C_D	0.09	0.07	0.11	0.07	0.06	0.14	0.15	0.10	0.16
L/D	4.21	4.70	3.36	5.61	5.92	4.15	4.09	4.79	3.99

In Table V: Base represents the basic shape, A represents the deformed shape A, B represents the deformed shape B, C_A represents the axial force coefficient of HGVs, C_N represents the normal force coefficient of HGVs, C_L represents the lift force coefficient of HGVs, C_D represents the drag force coefficient of HGVs, and L/D represents the lift-to-drag ratio of HGVs.

quality for the deformed model with the traditional control volume is 0.4947% and the descend range of the minimum mesh quality is 95.93%. The results show that there is almost no loss of mesh quality for the border-based FFD modeling method, which is superior to the traditional FFD modeling method.

FIGURE 19. The comparative of the pressures contours on the windward sides: (a) basic lifting body and deformed lifting body A, (b) basic lifting body and deformed lifting body B, (c) basic blended wing body and deformed blended wing body A, (d) basic blended wing body and deformed blended wing body B, (e) basic waverider body and deformed waverider body A, (f) basic waverider body and deformed waverider body B.
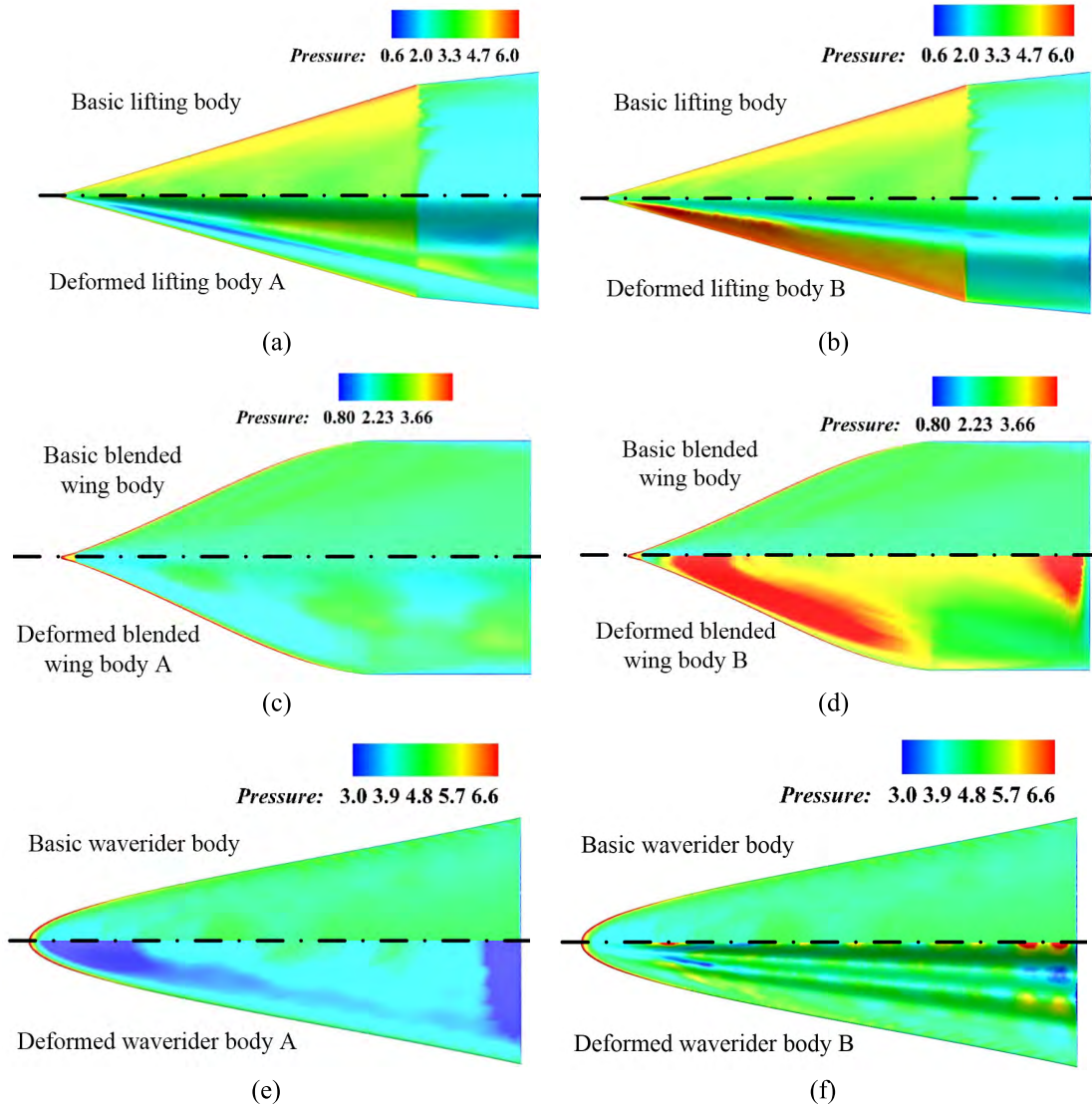
Fig. 12 shows the contours of the mesh quality of the deformed models and basic model obtained from different control lattices. Similar to the results in Fig. 10(a), there are several regions with low mesh quality and geometric discontinuities for the traditional control volume, as shown in Fig. 12(a) in the red boxes. In contrast, the mesh elements are better maintained by the border-based control surface, even in the regions that exhibit mesh distortion in the traditional control volume, as shown in Fig. 12(b) in the blue boxes. In addition, the highly consistent of the contours in Fig. 12(b) and Fig. 12(c) indicates that the mesh quality of the border-based FFD modeling method is in accordance with the basic model. The contours of the mesh quality demonstrate that a more robust deformation model can be obtained when using the border-based control surface; the mesh quality is high and the model has good geometric continuity.

C. MODELING CASES
The previous analysis demonstrated the superiorities of the border-based FFD modeling method. In order to illustrate the applicability of the proposed method, we apply it to the lifting body and two other typical HGV shapes, namely the blended wing body and the waverider body, as shown in Fig. 13.

There are two reasons for choosing the three typical HGV shapes; first, they represent commonly researched aerodynamic shapes of HGVs, including the lifting body, blended wing body, and waverider body. Second, all shapes have in common the common geometric feature of the windward side; lifting body has an external convex surface, blended wing body has a plane surface, and waverider body has an internal concave surface.

Based on the FFD modeling procedure (Fig. 6), we create the border-based control surfaces for different windward

sides of three HGVs, as shown in Fig. 14. The number of control points is $30 \times 20 (\vec{S} \times \vec{U})$ for all the border-based control surfaces, and the design control points only have one displacement change in $\vec{T}$ direction. During the FFD modeling of three HGVs, we can create various deformed results by choosing different positions and displacement changes of design control points. Under the constraints of the design requirements, only the smooth deformation along the streamline of the incoming flow can be created in this study.

For simplicity, we list two representative deformation results A and B for each shape. The models of basic lifting body and its two deformed results A and B are shown in Fig. 15, and the contours of the Y coordinates on the windward sides are appended to analyze the deformation degree.

The models of basic blended wing body and its two deformed results A and B are shown in Fig. 16, and the contours of the Y coordinates on the windward sides are appended to analyze the deformation degree.

The models of basic waverider body and its two deformed results A and B are shown in Fig. 17, and the contours of the Y coordinates on the windward sides are appended to analyze the deformation degree.

In order to analyze the deformation degree, the comparative contours of the Y coordinates on the windward sides are shown in Fig. 18. In all pictures, the contours of basic HGVs are shown on the top half and the contours of the deformed HGVs are shown on the bottom half.

As shown in Figures 15~18, all three HGVs can obtain favorable deformation results. This border-based FFD modeling method does not only provide a wide design space for the HGVs but also ensure good geometric continuity, even for large deformation.

D. SIMULATIONS

In order to verify the border-based FFD modeling method can provide effective support for the aerodynamic design of the HGV, we perform some aerodynamic simulations of the basic HGVs and deformed HGVs. During the simulation, the condition of the incoming flow is a free stream with the flight height of $H = 40\ km$, a Mach number of $Ma = 8$, and an angle of attack of $\alpha = 8°$. Based on the Euler equation, the simulation results were demonstrated through the axial force coefficient, normal force coefficient, lift force coefficient, drag force coefficient, and the lift-to-drag ratio of HGVs, as shown in Table 5.

By contrast, the differences of aerodynamic results between the basic HGV and corresponding deformed HGVs are significantly. The lift-to-drag ratio of L/D is a mainly index to reflect the aerodynamic performance of the HGV shape, and we can see the three HGVs all have the more superior deformed results of the L/D than the basic models.

In order to analyze the aerodynamic results in more detail, the comparisons of the pressure contours on the windward sides are presented in Fig. 19. From these figures, we can see the pressure on deformed HGVs (on the bottom half of each

figure) are obviously different with the basic HGVs (on the top half of each figure), so the aerodynamic performances are changed significantly by the border-based FFD modeling method.

All the results illustrate that the border-based FFD modeling method is better suited for parametric modeling and aerodynamic design of HGVs than the traditional method. The improvement of the L/D for each HGV illustrate that a wider design space and better support can be achieved by using this border-based FFD modeling method.

VI. CONCLUSION

In this study, a border-based FFD modeling method was proposed to ensure the FFD method can be suitable for parametric modeling and design of HGVs. The FFD control lattice was simplified; the dimensions of the control lattice were reduced from 3 to 2 and the displacement changes of the control points were limited to one direction. The boundary of the traditional control lattice was transformed into the border of windward side. By comparison, the border-based FFD modeling method reduced the complexity of computation, increased the efficiency of operation and had good geometric continuity.

Results of the robustness test of the deformed windward side demonstrated that the border-based FFD modeling method could create a more robust deformed model with high mesh quality and good geometric continuity. The applicability of the border-based FFD modeling method was validated by modeling three typical HGV shapes and simulating their aerodynamic performances. All three HGVs have the superior deformed results of the L/D than the basic shapes.

The main goal of this study was to provide better support for FFD modeling of the HGV. The high efficiency, wide design space and well applicability of the border-based FFD modeling method will allow researcher to achieve better design of the aerodynamic shape of the HGV. In follow-up work, more advanced parametric method will be developed and the concepts of this study will be extended to other related researches.

REFERENCES

[1] B. Zhang, T. Yang, Y. Ma, Z. Feng, and J. Ge, "Fast computation of hypersonic gliding lifting body aerodynamic based on configuration parameters," in *Proc. 7th Int. Conf. Intell. Hum.-Mach. Syst. Cybern.*, Aug. 2015, pp. 194–197.

[2] W. Huang, L.-Q. Li, L. Yan, and T.-T. Zhang, "Drag and heat flux reduction mechanism of blunted cone with aerodisks," *Acta Astron.*, vol. 138, pp. 168–175, Sep. 2017.

[3] D. Dirkx and E. Mooij, "Optimization of entry-vehicle shapes during conceptual design," *Acta Astronaut*, vol. 94, no. 1, pp. 198–214, 2014.

[4] S.-B. Li, Z.-G. Wang, G. N. Barakos, W. Huang, and R. Steijl, "Research on the drag reduction performance induced by the counterflowing jet for waverider with variable blunt radii," *Acta Astronaut*, vol. 127, pp. 120–130, Oct./Nov. 2016.

[5] F. Massobrio, R. Viotto, M. Serpico, A. Sansone, M. Caporicci, and J.-M. Muylaert, "EXPERT: An atmospheric re-entry test-bed," *Acta Astronautica*, vol. 60, no. 12, pp. 974–985, 2007.

[6] X. Guan, "Supersonic wing–body two-level wave drag optimization using extended far-field composite-element methodology," *AIAA J.*, vol. 52, pp. 981–990, Apr. 2014.

[7] F. Ding, J. Liu, C.-B. Shen, and W. Hunag, "Novel inlet–airframe integration methodology for hypersonic waverider vehicles," *Acta Astronautica*, vol. 111, pp. 178–197, Jun./Jul. 2015.

[8] D. A. Masters, N. J. Taylor, T. Rendall, C. B. Allen, and D. J. Poole, "Review of aerofoil parameterisation methods for aerodynamic shape optimisation," in *Proc. 53rd AIAA Aerosp. Sci. Meeting*, Kissimmee, FL, USA, 2015, p. 0761.

[9] C. Gong, Y. X. Xu, W. W. Zheng, and X. Bin, "Concept design of a near-space high L/D ratio glide vehicle," *Flight Dyn.*, vol. 34, no. 5, pp. 44–48, 2016.

[10] C. C. Morris, D. L. Allison, J. A. Schetz, R. K. Kapania, and C. Sultan, "Parametric geometry model for design studies of tailless supersonic aircraft," *J. Aircraft*, vol. 51, no. 5, pp. 1455–1466, 2014.

[11] T.-T. Zhang, Z.-G. Wang, W. Huang, and L. Yan, "A review of parametric approaches specific to aerodynamic design process," *Acta Astronautica*, vol. 145, pp. 319–331, Apr. 2018.

[12] J. Griessmair and W. Purgathofer, "Deformation of solids with trivariate B-splines," *Proc. Eurographics*, vol. 21, pp. 137–148, Sep. 1989.

[13] W. Zhang, L. Zhao, T. Gao, and S. Cai, "Topology optimization with closed B-splines and Boolean operations," *Comput. Methods Appllied Mech. Eng.*, vol. 315, pp. 652–670, Mar. 2017.

[14] L. Piegl and W. Tiller, *The NURBS Book*. Berlin, Germany: Spinger, 1995.

[15] B. Kulfan, "A universal parametric geometry representation method— 'CST,'" in *Proc. 45th AIAA Aerosp. Sci. Meeting Exhibit*, Reno, Nevada, 2007, p. 62.

[16] H. Sobieczky, "Parametric airfoils and wings," in *Recent Development of Aerodynamic Design Methodologies* (Notes on Numerical Fluid Mechanics), vol. 68. Verlag, Germany: Vieweg, 1998, pp. 71–88.

[17] R. M. Hicks and P. A. Henne, "Wing design by numerical optimization," *J. Aircraft*, vol. 15, no. 7, pp. 407–412, 1978.

[18] T. C. S. Rendall and C. B. Allen, "Unified fluid–structure interpolation and mesh motion using radial basis functions," *Int. J. Numer. Methods Eng.*, vol. 74, pp. 1519–1559, Jun. 2008.

[19] T. W. Sederberg and S. R. Parry, "Free-form deformation of solid geometric models," *ACM SIGGRAPH Comput. Graph.*, vol. 20, no. 4, pp. 151–160, 1986.

[20] B. Zhang, Z. Feng, T. Yang, B. Xu, and X. Sun, "Integrated improvement of the elasticity-based mesh deformation method based on robust parameters and mesh quality," *Part G, J. Aerosp. Eng.*, to be published. doi: 10.1177/0954410018790887.

[21] H. J. Lamousin and W. N. Waggenspaek, "NURBS-based free-form deformations," *IEEE Comput. Graph. Appl.*, vol. 14, no. 6, pp. 59–65, Nov. 1994.

[22] S. Coquillart, "Extended free-form deformation: A sculpting tool for 3D geometric modeling," *Comput. Graph.*, vol. 24, no. 4, pp. 187–196, 1990.

[23] W. M. Hsu, J. F. Hughes, and H. Kaufman, "Direct manipulation of free-form deformation," *ACM Siggraph Comput. Graph.*, vol. 26, no. 2, pp. 177–184, 1992.

[24] J. Feng, L. Ma, and Q. Peng, "A new free-form deformation through the control of parametric surfaces," *Comput. Graph.*, vol. 20, no. 4, pp. 531–539, 1996.

[25] S.-H. Yoon and M.-S. Kim, "Sweep-based freeform deformations," *Comput. Graph. Forum*, vol. 25, no. 3, pp. 487–496, 2006.

[26] H. Gagnon and D. W. Zingg, "Two-level free-form deformation for high-fidelity aerodynamic shape optimization," in *Proc. 12th AIAA Aviation Technol., Intergration, Oper. Conf. (ATIO)*, Indianapolis, IN, USA, 2012, p. 5447.

[27] D. Koo and D. W. Zingg, "Investigation into aerodynamic shape optimization of planar and nonplanar wings," *AIAA J.*, vol. 56, pp. 250–263, Jul. 2018.

[28] L. Piegl, "On NURBS: A survey," *IEEE Comput. Graph. Appl.*, vol. 1, no. 1, pp. 55–71, Jan. 1991.

[29] Z. Xu, J. Xia, and Y. Gao, "Continuous adjoint approach to aerodynamic optimization on 3D unstructured grids," *J. Nanjing Univ. Aeronaut. Astronautics*, vol. 47, no. 1, pp. 145–152, 2015.

[30] R. MacCracken and K. I. Joy, "Free-form deformations with lattices of arbitrary topology," in *Proc. 23rd Annu. Conf. Comput. Graph. Interact. Techn.*, 1996, pp. 181–188.

[31] D. Bechmann, Y. Bertrand, and S. Thery, "Continuous free form deformation," *Comput. Netw. ISDN Syst.*, vol. 29, pp. 1715–1725, Oct. 1997.

[32] P. M. Knupp, "Algebraic mesh quality metrics for unstructured initial meshes," *Finite Elements Anal. Des.*, vol. 39, pp. 217–241, Jan. 2003.
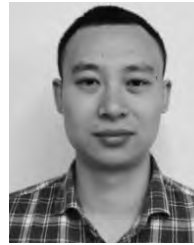
BIN ZHANG was born in Binzhou, Shandong, China, in 1990. He received the B.S. degree in aerospace engineering and the M.S. degree in aeronautical and astronautical science and technology from the National University of Defense Technology, Changsha, China, in 2013 and 2016, respectively, where he is currently pursuing the Ph.D. degree in aeronautical and astronautical science and technology.

His research interests include aerodynamic shape design and optimization of flight vehicles.

ZHIWEI FENG was born in Linfen, Shanxi, China, in 1984. He received the B.S. degree in aerospace engineering, the M.S. degree in aeronautical and astronautical science and technology, and the Ph.D. degree in mechanics from the National University of Defense Technology, Changsha, China, in 2006, 2008, and 2014, respectively, where he has been a Lecturer, since 2014.

His research interests include aerodynamic design and multi-objective optimization of flight vehicles.

BOTING XU was born in Shangrao, Jiangxi, China, in 1992. She received the B.S. degree in aerospace engineering and the M.S. degree in aeronautical and astronautical science and technology from the National University of Defense Technology, Changsha, China, in 2013 and 2016, respectively, where she is currently pursuing the Ph.D. degree in aeronautical and astronautical science and technology.

Her research interests include dynamic simulation and control of flight vehicles.

TAO YANG was born in Changde, Hunan, China, in 1962. He received the B.S. and M.S. degrees in solid rocket engine technology from the National University of Defense Technology, Changsha, China, in 1983 and 1989, respectively, and the Ph.D. degree in ballistics from the Nanjing University of Science and Technology, Nanjing, China, in 1992.

From 1992 to 1994, he was a Lecturer with the National University of Defense Technology, where he was an Associate Professor, from 1994 to 2001, and he has been a Professor, since 2001. His research interests include overall design and optimization of flight vehicles, and aerospace propulsion theory and engineering.

● ● ●